Chymase Inhibition Attenuates Kidney Fibrosis in a Chronic Mouse Model of Renal Ischemia-Reperfusion Injury

Sakura Kure , Hiroe Toba , Denan Jin * , Akira Mima , Shinji Takai

Posted Date: 12 March 2025

doi: 10.20944/preprints202503.0870.v1

Keywords: chymase; mast cells; chymase inhibitor; angiotensin II; transforming growth factor (TGF)-β1

Article

Chymase Inhibition Attenuates Kidney Fibrosis in a Chronic Mouse Model of Renal Ischemia-Reperfusion Injury

Sakura Kure [1,2], Hiroe Toba [1,3], Denan Jin [1,*], Akira Mima [2] and Shinji Takai [1]

[1] Department of Pharmacology, Osaka Medical and Pharmaceutical University, Takatsuki-City, Osaka 569-8686, Japan

[2] Department of Nephrology, Osaka Medical and Pharmaceutical University, Takatsuki-City, Osaka 569-8686, Japan

[3] Department of Clinical Pharmacology, Division of Pathological Sciences, Kyoto Pharmaceutical University, 1 Misasagi Shichono-cho, Yamashina-ku, Kyoto 607-8412, Japan

* Correspondence: denan.jin@ompu.ac.jp; Tel.: +81-72-683-1221

Abstract: Although various factors contribute to the transition from acute kidney injury (AKI) to chronic kidney disease (CKD), no clinically effective pharmacological treatment has been established. We investigated whether chymase inhibition is effective in preventing renal fibrosis, a key process in the transition from AKI to CKD. Male BALB/c mice were subjected to unilateral ischemia-reperfusion (I/R) injury, and TY-51469, a chymase-specific inhibitor, was administered intraperitoneally at a dose of 10 mg/kg/day for 6 weeks. The 45-minute ischemic period followed by 6 weeks of reperfusion resulted in severe renal atrophy. Renal fibrosis was particularly pronounced at the transition region between the cortex and medulla in placebo-treated mice. Expression of mouse mast cell protease 4 (MMCP-4, a mouse chymase) mRNA, number of chymase-positive mast cells, and fibrosis-related factors, such as transforming growth factor (TGF)-β1 and collagen I were all significantly increased in I/R-injured kidneys. However, treatment with TY-51469 significantly suppressed fibrosis formation, along with inhibition of renal chymase and TGF-β1 expression. These findings suggest that chymase inhibition may be a potential therapeutic strategy for preventing the transition from AKI to CKD by reducing fibrosis.

Keywords: chymase; mast cells; chymase inhibitor; angiotensin II; transforming growth factor (TGF)-β1

1. Introduction

Acute kidney injury (AKI) is a significant risk factor for chronic kidney disease (CKD) and end-stage renal disease (ESRD). Various common pathological conditions can lead to AKI, including hemorrhage, fluid loss, circulatory failure, cardiovascular surgery, shock, and transplant surgery, resulting in a rapid decline in kidney function [1]. For a long time, AKI was considered a temporary condition, and it was believed that patients who recovered from AKI through medical treatment would not experience long-term complications. However, recent evidence suggests that AKI plays a crucial role in the progression to CKD. For example, even though AKI patients successfully recover from the acute phase and are discharged from the hospital, studies have reported that up to 50% of them develop CKD within a few years [2]. This suggests that kidney damage caused by AKI might persist despite aggressive treatment. Indeed, even when serum creatinine levels return to baseline, structural damage to the kidney can persist for a long time, potentially leading to the development of CKD [3–5]. Although the mechanisms underlying the transition from AKI to CKD are not yet fully understood, factors such as endothelial dysfunction [6,7], interstitial inflammation ([8,9], fibrosis

 doi:10.20944/preprints202503.0870.v1

[10,11], and tubular epithelial injury [12,13] are thought to contribute to this progression. Endothelial dysfunction can lead to oxygen deficiency in kidney tissue, resulting in mitochondrial dysfunction in various cell types and damage to renal tubular epithelial cells, ultimately triggering sterile interstitial inflammation. Simultaneously, repair mechanisms are activated in response to this inflammation. However, excessive repair following AKI can lead to renal fibrosis, further damaging normal kidney structure and promoting the progression from AKI to CKD.

Recent studies have highlighted possible molecular mechanisms involved in these inflammatory and fibrotic processes following AKI. For example, inflammatory mediators such as tumor necrosis factor-alpha (TNF-α), interleukin-1 beta (IL-1β), and interleukin-6 (IL-6) are produced by the renal tubular epithelium after ischemia-reperfusion (I/R) injury [14–16]. Additionally, a significant increase in transforming growth factor-beta 1 (TGF-β1), a key mediator of fibrosis, has been observed in the cytoplasm of interstitial cells in mouse models of I/R injury [17]. These findings indicate that activation of both, inflammation-related factors and fibrosis-related mediators, is critical in the transition from AKI to CKD. Although some causative factors in the transition from AKI to CKD after I/R injury in animal models have been identified, effective pharmacological therapies for preventing this progression have not yet been established in clinical practice.

Recently, mast cell-derived chymase, a novel component of the renin-angiotensin system (RAS), has attracted significant attention. Under certain conditions, such as ischemia or inflammation, chymase is released through degranulation, and functions similar to angiotensin-converting enzyme (ACE), cleaving angiotensin I (Ang I) into angiotensin II (Ang II) [18]. In addition to its role in Ang II generation, chymase can also activate latent TGF-β1, converting it into its active form [19]. Ang II is a well-known pro-inflammatory molecule involved not only in hypertension, but also in fibrosis of various organs. Given these unique properties of chymase, we investigated its expression in the kidney following I/R injury, and evaluated whether long-term treatment with a chymase-specific inhibitor could prevent renal fibrosis in a mouse model of unilateral renal I/R injury.

2. Results

2.1. Procedure for creating the I/R model and subsequent changes in KW to BW ratio

Figure 1A shows a photograph of the left kidney of an anesthetized mouse after renal ischemia for 45 minutes. Renal ischemia was induced by blocking both arterial and venous blood flow using an arterial clamp on the left renal pedicle. As seen in Figure 1A, the renal surface turned dark purple 45 minutes after pedicle clamping, indicating stagnant blood flow. However, a few seconds after removing the clamp, the kidney turned light red (Figure 1B), signifying restoration of blood flow.

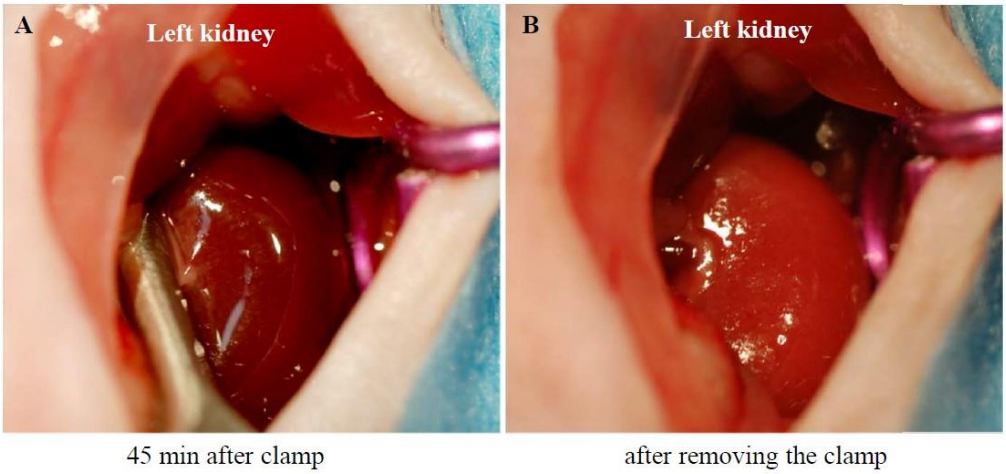

Figure 1. Changes in kidney surface color during ischemia and reperfusion.

 doi:10.20944/preprints202503.0870.v1

As shown in Figure 2D, the body weight (BW) of each experimental group was approximately the same before the start of the experiments. However, BW increased to some extent in all the experimental groups 6 weeks after surgery. Figure 2A shows representative photographs of the right and left kidneys 6 weeks after the sham operation. As seen in the photograph, there was not much difference in size between the two kidneys. Similarly, the kidney weight (KW) to BW ratio showed no significant difference between the left and right kidneys 6 weeks after the sham operation (Figure 2E). However, six weeks after the I/R injury, the ischemic left kidney was significantly shrunken compared to the contralateral and sham-operated left kidneys (Figure 2B). When KW was adjusted for BW, the KW/BW ratio of the ischemic left kidney was significantly lower than that of contralateral and sham-operated kidneys (Figure 2E). Interestingly, the contralateral healthy right kidney in the I/R mice seemed to undergo compensatory hypertrophy, resulting in a significantly higher KW/BW ratio as compared to the sham-operated right kidney (Figure 2E). As seen in Figures 2C and 2E, the KW/BW ratio of the left I/R kidney in TY-51469-treated mice was similar to that of the placebo-treated group. However, the compensatory mechanisms in TY-51469-treated mice appeared to be less severe, as shown by the fact that the KW/BW ratio of the right kidney in these mice did not differ significantly from that of the sham-operated right kidney (Figure 2E).

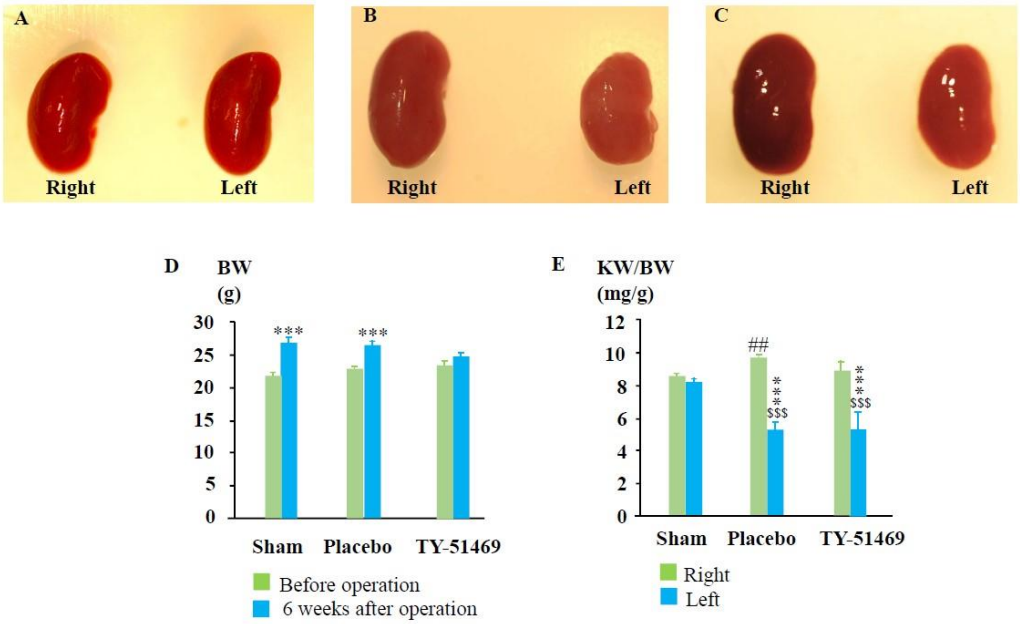

Figure 2. Changes in body weight and kidney weight 6 weeks after the sham operation or I/R injury. Representative photographs of the right and left kidneys 6 weeks after surgery from a sham-operated mouse (A), and from I/R mice treated with placebo (B) and TY-51469 (C). (D): Changes in body weight 6 weeks after the sham operation or after the I/R injury. (E): Changes in the ratio of kidney weight to body weight 6 weeks after the sham operation or I/R. $^{\$\$\$}P < 0.001 vs the non-ischemic contralateral kidney. $^{\#\#}P < 0.01$ vs. the sham-operated right kidney. ***P < 0.001 vs. the sham-operated left kidney.

2.2. Characteristics of renal fibrosis after I/R

As shown in Figure 3A, the sham-operated kidney exhibited normal histology, with no significant renal fibrosis.

 doi:10.20944/preprints202503.0870.v1

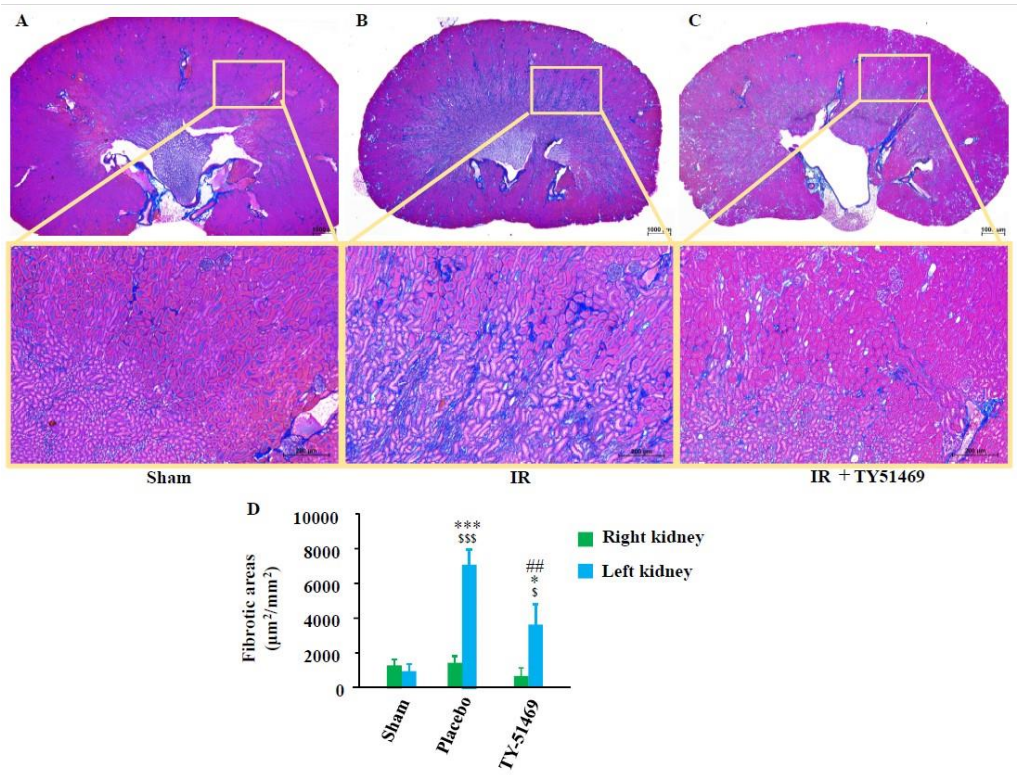

Figure 3. Azan-Mallory staining and quantification of renal fibrotic areas. Representative images of Azan-Mallory-stained cross-sections from a sham-operated mouse (A), and from an I/R mouse treated with placebo (B) and TY-51469 (C). The blue-stained areas represent collagen deposition. (D): Quantification of renal interstitial fibrotic areas in cross-sections of kidneys from sham-operated mice or I/R mice treated with placebo and TY-51469. $^{\$}P < 0.05$, $^{\$\$\$}P < 0.001$ vs. the non-ischemic contralateral kidney. $^{*}P < 0.05$, $^{***}P < 0.001$ vs. the sham-operated left kidney. $^{\#\#}P < 0.01$ vs. the placebo-treated left kidney.

However, in 6-week I/R injured placebo-treated kidneys, there were remarkably more blue-stained areas at the transition region between the cortex and medulla (Figure 3B), and the calculated fibrotic area in the placebo-treated group was significantly larger compared to that in the sham-operated group (Figure 3D). On the other hand, TY-51469 treatment commencing one day after the I/R injury significantly reduced fibrosis in the I/R kidney (Figures 3C,D).

2.3. Changes in chymase-positive mast cells in renal fibrosis areas after I/R

Figure 4A shows representative toluidine blue staining for identification of mast cells in a sham-operated kidney 6 weeks after surgery. As seen in this section, few mast cells were observed in the non-injured healthy kidney. However, mast cells accumulated in the fibrotic region of the kidney 6 weeks after I/R (Figure 4B), with a significant increase in the mean number of mast cells in the I/R-injured kidney—by dozens of times—compared to sham-operated non-injured kidneys (Figure 4D). Figure 4C shows mast cell distribution in the I/R kidney from a mouse treated with TY-51469 for 6 weeks. As indicated in Figure 4D, although the number of mast cells in the TY-51469-treated I/R kidney was still significantly higher than that in the sham-operated group, TY-51469 treatment significantly reduced mast cell accumulation compared to the non-treated placebo group (Figure 4D).

 doi:10.20944/preprints202503.0870.v1

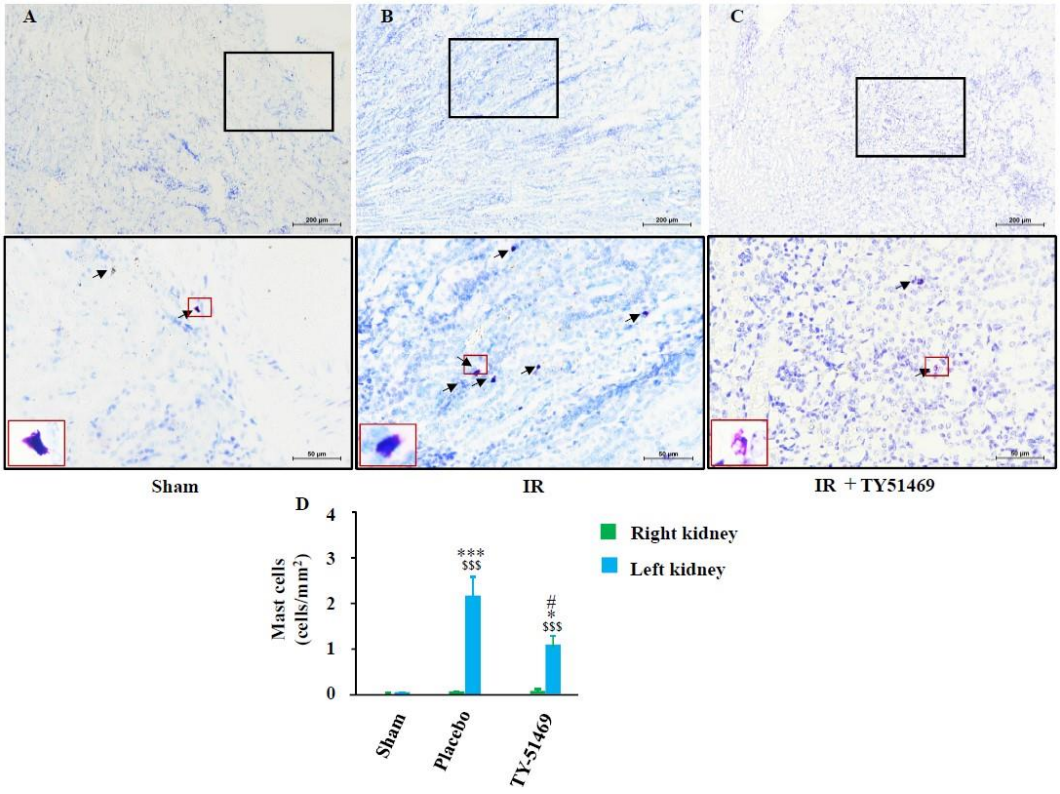

Figure 4. Toluidine blue staining and quantification of mast cells. Representative images of toluidine blue-stained cross-sections of the kidneys of a sham-operated mouse (A), and I/R mouse treated with placebo (B) and TY-51469 (C). Mast cells are indicated by black arrows. (D): Quantification of mast cells in cross-sections of kidneys from sham-operated mice and I/R mice treated with placebo and TY-51469. $^{\$\$\$}P < 0.001 vs. the non-ischemic contralateral kidney. *P < 0.05, ***P < 0.001 vs. the sham-operated left kidney. $^{\#}P < 0.05$ vs. the placebo-treated left kidney.

Figure 5A shows representative chymase (mouse mast cell protease 4, MMCP-4) immunostaining in a sham-operated kidney 6 weeks after surgery. Similar to Figure 4A (toluidine blue staining), few chymase-positive cells were observed in the non-injured healthy kidney (Figure 5A). However, chymase -positive cells increased dramatically in the fibrotic region of the kidney 6 weeks after I/R (Figure 5B), and their distribution pattern closely resembled that of the mast cells in Figure 4B. Since Figures 4B and 5B present adjacent serial sections, these findings suggest that chymase is primarily expressed in mast cells. Compared to the sham-operated group, the number of chymase -positive cells significantly increased in I/R-injured kidneys (Figure 5D), while continued TY-51469 treatment for 6 weeks largely reduced chymase -positive cell expression (Figure 5C,D).

 doi:10.20944/preprints202503.0870.v1

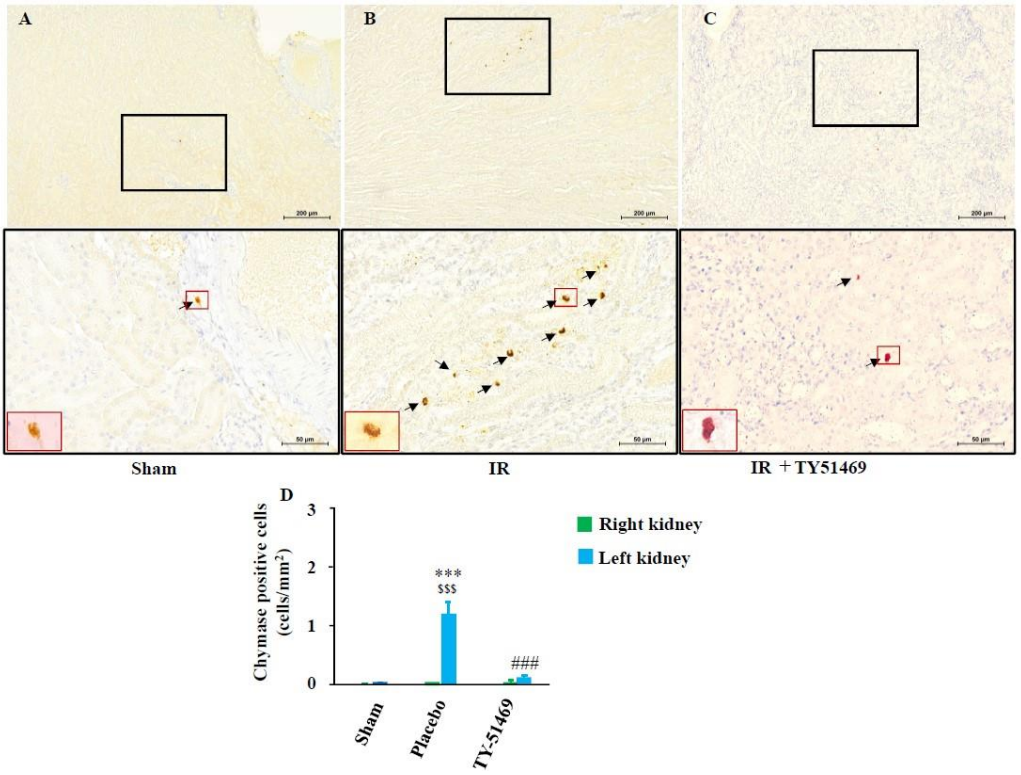

Figure 5. Chymase immunostaining and quantification of chymase-positive cells. Representative images of chymase-immunostained cross-sections from a sham-operated mouse (A), and from I/R mice treated with placebo (B) and TY-51469 (C). Chymase-positive cells are indicated by black arrows. (D): Quantification of chymase-positive cells in cross-sections of kidneys from sham-operated mice and I/R mice treated with placebo and TY-51469. $^{\$\$\$}P < 0.001 vs. the non-ischemic contralateral kidney. ***P < 0.001 vs. the sham-operated left kidney. $^{\#\#\#}P < 0.001$ vs. the placebo-treated left kidney.

2.4. Changes in gene expression levels of MMCP-4, TGF-β1, and collagen I after I/R

Figure 6A shows MMCP-4 mRNA expression levels 6 weeks after surgery. As seen in the bar graph in Figure 6A, MMCP-4 expression in I/R-injured kidneys was significantly higher compared to non-injured sham-operated left kidneys and contralateral kidneys. However, MMCP-4 expression in I/R-injured kidneys was significantly suppressed by TY-51469 treatment. Fibrosis-related factors, such as TGF-β1 and collagen I, were also significantly elevated in I/R-injured kidneys compared to the sham-operated left kidney or the contralateral uninjured kidney. These elevations were significantly suppressed by TY-51469 treatment (Figure 6B,C).

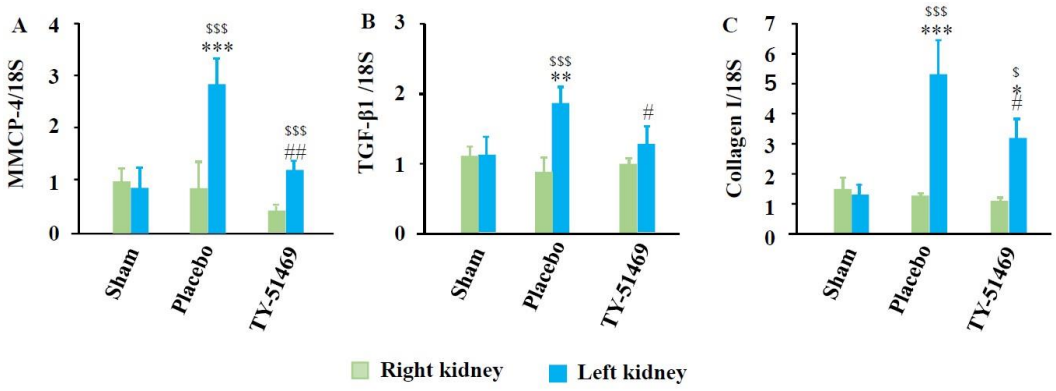

Figure 6. Changes in MMCP-4, TGF-β1, and collagen mRNA expression 6 weeks after the sham operation or I/R. $^{\$}P < 0.05$, $^{\$\$\$}P < 0.001$ vs. the non-ischemic contralateral kidney. *P < 0.05, **P < 0.01, ***P < 0.001 vs. the sham-operated left kidney. $^{\#}P < 0.05$, $^{\#\#}P < 0.01$ vs. the placebo-treated left kidney.

 doi:10.20944/preprints202503.0870.v1

2.5. Correlation among renal MMCP-4, TGF-β1 and collagen I gene expression levels after I/R

As seen in Figure 7A, the correlation coefficient (r) between MMCP-4 and TGF-β1 was 0.443, with a p-value of less than 0.05, indicating a close relationship between these factors. A significant correlation was also observed between mRNA expression levels of MMCP-4 and collagen I, as well as between TGF-β1 and collagen I.

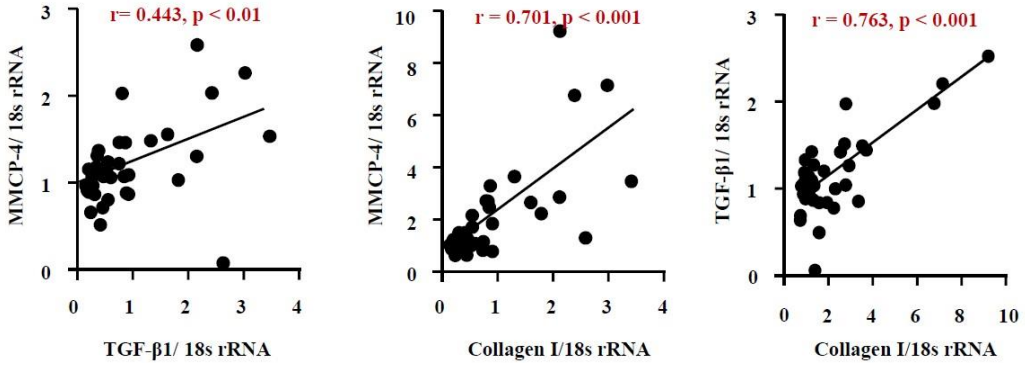

Figure 7. Linear regression analyses of mRNA expression levels of MMCP-4, TGF-β1, and collagen I. Correlations were observed between MMCP-4 and TGF-β1 mRNA levels (A), MMCP-4 and collagen I mRNA levels (B), and TGF-β1 and collagen I mRNA levels (C) in all the examined kidneys 6 weeks after surgery.

3. Discussion

Both unilateral and bilateral I/R injury models are commonly used to mimic clinical ischemic kidney injury in medical research. A certain duration of ischemia causes oxygen deprivation in kidney tissues, leading to damage in various kidney cells. While subsequent reperfusion restores oxygen supply, the process might exacerbate kidney damage due to the excessive production of reactive oxygen species [20,21]. I/R injury is characterized by endothelial dysfunction, cell death via apoptosis and necrosis, and immune cell accumulation, ultimately leading to progressive renal fibrosis. This excessive repair mechanism disrupts the normal renal structure and gradually progresses to CKD [22,23]. In this study, we employed a unilateral renal I/R model in mice to investigate whether mast cell-derived chymase plays a role in kidney fibrosis over a 6-week observation period, since the dual-kidney I/R model has a high mortality rate and is unsuitable for long-term analysis of fibrosis [24]. As shown in Figure 2E, no significant difference in the KW/BW ratio between the left and right kidneys was observed 6 weeks after the sham operation. However, in placebo-treated I/R mice, significant atrophy of the ischemic left kidney was noted. Interestingly, the KW/BW ratio of the contralateral, non-ischemic right kidney was significantly higher in the placebo-treated group compared to the sham group (Figure 2E), suggesting the occurrence of compensatory hypertrophy due to long-term dysfunction of the ischemic left kidney in the placebo group. Similarly, the ischemic left kidney in TY-51469-treated mice also showed atrophy 6 weeks after I/R. However, unlike in placebo-treated mice, compensatory hypertrophy of the contralateral right kidney was significantly reduced, suggesting that TY-51469, a chymase-specific inhibitor, might mitigate the pathological changes in the ischemic kidney and improve renal function post-I/R. As a matter of fact, we found that the fibrotic area in the ischemic left kidney in the placebo-treated group was significantly increased compared to the sham-operated kidney, with fibrosis predominantly localized at the transition region between the cortex and medulla (Figure 3B,D). In contrast, long-term TY-51469 treatment effectively suppressed fibrosis following I/R injury (Figure 3C,D). These findings suggest that mast cell-derived chymase activation plays a crucial role in fibrosis during the long-term period after I/R injury in mice. Our observation that the number of mast cells and MMCP-4-positive cells in the placebo-treated ischemic left kidney were significantly increased compared to the sham-operated, non-ischemic kidney (Figures 4 and 5) supports this hypothesis. The distribution of both mast cells and MMCP-4-positive cells was also concentrated in the transition region between the

 doi:10.20944/preprints202503.0870.v1

cortex and medulla, where fibrosis was most prominent. Additionally, MMCP-4 mRNA expression was significantly elevated in the ischemic left kidney in the placebo-treated group compared to the sham-operated kidney. Since TY-51469 treatment suppressed both chymase-positive mast cell accumulation and MMCP-4 gene expression, which correlated with reduced fibrosis, it is likely that chymase activation indeed played a role in the pathogenesis of renal fibrosis in this model.

How does chymase activation contribute to fibrosis formation after I/R injury? Mice reportedly express several types of chymases, including mouse mast cell protease-1 (MMCP-1), MMCP-2, MMCP-3, and MMCP-4, each with distinct enzymatic properties [25]. Among them, MMCP-4 is functionally considered the most similar to human chymase, particularly in its ability to generate Ang II [26]. Ang II is known to promote superoxide production via NADPH oxidase (NOX) activation [27], leading to the release of pro-inflammatory cytokines such as TNF-α, IL-1β, and IL-6 through nuclear factor-kappa B (NF-κB) activation [28,29]. In addition to Ang II generation, chymase can activate latent TGF-β1 into its active form [19]. Since TNF-α, IL-1β, and IL-6 are all elevated following renal I/R injury [20,21], and TGF-β1 is considered a key pro-fibrotic factor involved in the transition from acute kidney injury (AKI) to CKD [22,23], inhibition of MMCP-4 by TY-51469 likely reduces the production of both inflammatory and fibrotic mediators, such as TNF-α and TGF-β1. These inhibitory effects of chymase might have contributed to the attenuation of fibrosis in this mouse unilateral I/R injury model.

4. Materials and Methods

4.1. Animals

Male BALB/c mice (SLC, Shizuoka, Japan) aged 6 weeks, weighing 18–22 g, were used. All experimental procedures were conducted in accordance with the guidelines of Osaka Medical and Pharmaceutical University for medical experiments, and were approved by the local institutional ethics committee (AM23-111). The mice were fed a standard diet, had free access to tap water, and were housed in a temperature-, humidity-, and light-controlled environment.

4.2. Creation of the unilateral renal I/R injury model

The renal I/R injury model was established under mixed anesthesia (0.3 mg/kg medetomidine, 4.0 mg/kg midazolam, and 5.0 mg/kg butorphanol tartrate). Briefly, mice were anesthetized via intraperitoneal injection (i.p.) of the mixed anesthetic and underwent midline incisions. The left renal pedicle was bluntly dissected, and an arterial clamp was applied for 45 minutes. During this period, the animals were maintained at a constant temperature (~37°C) and kept well-hydrated. After 45 minutes of ischemia, the clamp was removed, wounds were sutured, and the mice were allowed to recover. Sham-operated animals underwent the same surgical procedure without the ischemic insult.

4.3. Grouping and Sampling

The renal I/R injury model was induced in 12 mice, which were then divided into two groups: placebo-treated (n = 6) and TY-51469-treated (n = 6), respectively. TY-51469, a chymase-specific inhibitor, was administered intraperitoneally at a dose of 10 mg/kg once daily, starting one day after surgery and continuing until the end of the experiment. Sham operations were performed on an additional six mice. Six weeks after surgery, all 18 mice were sacrificed under pentobarbital overdose anesthesia, and both ischemic and normal kidneys were harvested and weighed. Each kidney was bisected longitudinally; one half was fixed in Carnoy's solution for histological, while the other half was frozen for biochemical examinations, respectively.

4.4. Reverse Transcriptio Polymerase Chain Reaction (RT-PCR)

RT-PCR was performed to assess the expression of MMCP-4 (a mouse chymase), TGF-β1, and collagen I in renal tissues using previously described methods [30]. Briefly, total renal RNA was

 doi:10.20944/preprints202503.0870.v1

extracted using Trizol reagent (Life Technologies, Rockville, MD, USA) and dissolved in RNase-free water (Takara Bio Inc., Otsu, Japan). One microgram of total RNA was transcribed into complementary DNA (cDNA) using Superscript VIRO (Invitrogen, Carlsbad, CA, USA). mRNA levels were then quantified by RT-PCR using a Stratagene Mx3000P system (Agilent Technologies, San Francisco, CA, USA) and TaqMan fluorogenic probes. RT-PCR primers and probes for MMCP-4, collagen I, TGF-β1, and 18S ribosomal RNA (rRNA) were designed by Roche Diagnostics (Tokyo, Japan). The primer sequences were as follows:

MMCP-4: Forward: 5′-ggcctgtaaaaactattggcatt-3′, Reverse: 5′-cacacagtagaggtcctccaga-3′
Collagen I: Forward: 5′-catgttcagctttgtggacct-3′, Reverse: 5′-gcagctgattgagggatgt-3′
TGF-β1: Forward: 5′-tggagcaacatgtggaactc-3′, Reverse: 5′-cagcagccggttaccaag-3′
18S rRNA: Forward: 5′-gcaattattccccatgaacg-3′, Reverse: 5′-gggacttaatcaacgcaagc-3′
The probe sequences were as follows:
MMCP-4: 5′-tccaggtc-3′
Collagen I: 5′-tcctgtc-3′
TGF-β1: 5′-ttcctggc-3′
18S rRNA: 5′-ttcccagt-3′
The mRNA levels of MMCP-4, collagen I, and TGF-β1 were normalized to those of 18S rRNA.

4.5. Histological Studies

Carnoy-fixed kidneys were embedded in paraffin, and 3-μm-thick serial cross-sections were prepared using a sliding microtome (LITORATOMU, REM-710, Yamato Koki Kogyo Ltd., Asagiri, Saitama, Japan). To assess renal fibrosis, the first section from each sample was stained with Azan-Mallory stain. Three areas per section were randomly selected at 200× magnification using a computerized morphometry system (NIS-Elements Documentation, v.3.07, Nikon, Tokyo, Japan). The average fibrotic area was then quantified using WinROOF2021, an image analysis software. To evaluate mast cell distribution, the second section from each sample was stained with toluidine blue. Briefly, after deparaffinization with remosol (Wako Pure Chemicals, Osaka, Japan), sections were immersed in 0.5% toluidine blue solution (pH 4.8) for approximately 15 minutes, fractionated with 0.5% glacial acetic acid solution, and mounted after drying. To determine chymase distribution, immunohistochemical staining was performed on the third serial section using an anti-murine mast cell protease-4 (anti-MMCP-4) antibody (ab92368, Abcam, Cambridge, UK), following a previously described protocol [31]. Briefly, to suppress endogenous peroxidase activity and nonspecific binding, deparaffinized sections were sequentially incubated with 3% hydrogen peroxide and a protein-blocking solution, each for 5 minutes, at room temperature. The sections were then incubated overnight at 4°C with the diluted primary antibody (1:100), followed by detection using a labeled streptavidin-biotin peroxidase kit (Dako LSAB kit, Carpinteria, CA, USA) and 3-amino-9-ethylcarbazole for color development. Sections were lightly counterstained with hematoxylin and mounted with cover glasses. Following staining, mast cell and chymase-positive cell counts were evaluated under a computerized morphometry system, and the number of cells per unit area was compared between experimental groups.

4.6. Statistical analysis

All numerical data are expressed as the mean ± standard error of the mean (SEM). Statistically significant differences among multiple groups were assessed using one-way analysis of variance (ANOVA) followed by post hoc analysis (Fisher's test). A P value of <0.05 was considered statistically significant. Correlations were analyzed using Pearson's correlation coefficient.

5. Conclusions

In conclusion, chymase gene expression, the number of chymase-positive mast cells, and the fibrosis-related factor TGF-β1 were all significantly elevated in kidneys with I/R injury. Treatment

 doi:10.20944/preprints202503.0870.v1

with the chymase-specific inhibitor TY-51469 reduced chymase expression and TGF-β1 levels, resulting in significant improvement in fibrosis formation. These findings indicate that mast cell-derived chymase plays a role in the pathogenesis of renal fibrosis following I/R injury in mice. Furthermore, inhibition of chymase might represent a potential therapeutic strategy to prevent the transition from AKI to CKD.

Author Contributions: S.K. and D.J. conceived and supervised the study and wrote the manuscript. S.K., H.T., and S.T. performed histological and gene expression analyses. A.M. reviewed the manuscript. All authors have read and approved the final version of the manuscript.

Acknowledgments: This study was supported in part by Grants-in-Aid 17K09741, 24590336, 21590295, 15590240, 13670102, and 20K08601 for Scientific Research (C) from the Ministry of Education, Science, Sports, and Culture, Japan

Conflicts of Interest: The authors declare no conflicts of interest.

References

1. Bonventre, J.V.; Weinberg, J.M. Recent advances in the pathophysiology of ischemic acute renal failure. *J Am Soc Nephrol* **2003**, 14, 2199-2210.
2. Bucaloiu, I.D.; Kirchner, H.L.; Norfolk, E.R.; Hartle, J.E.; Perkins, R.M. Increased risk of death and de novo chronic kidney disease following reversible acute kidney injury. *Kidney Int.* **2012**, 81, 477-485.
3. Li, Z.; Li. N. Epigenetic modification drives acute kidney injury-to-chronic kidney disease progression. *Nephron* **2021,** 145, 737-747.
4. Liu, J.; Kumar, S.; Dolzhenko, E.; Alvarado, G.F.; Guo, J.; Lu. C.; Chen, Y.; Li, M.; Dessing, M.C.; Parvez, R.K.; Cippà, P.E.; Krautzberger, A.M.; Saribekyan, G.; Smith, AD.; McMahon, A.P. Molecular characterization of the transition from acute to chronic kidney injury following ischemia/reperfusion. *JCI Insight.* **2017**, 2, e94716.
5. Liu, B.C.; Tang, T.T.; Lv, L.L.; Lan, H.Y. Renal tubule injury: a driving force toward chronic kidney disease, *Kidney Int.* **2018,** 93, 568–579.
6. Basile, D.P. The endothelial cell in ischemic acute kidney injury: Implications for acute and chronic function. *Kidney Int.* **2007,** 72, 151–156.
7. Basile, D.P.; Collett, J.A.; Yoder, M.C. Endothelial colony-forming cells and pro-angiogenic cells: Clarifying definitions and their potential role in mitigating acute kidney injury. *Acta. Physiol. Oxf. Engl.* **2018**, 222, e12914.
8. Anders, H.J.; Schaefer, L. Beyond Tissue Injury—Damage-Associated Molecular Patterns, Toll-Like Receptors, and Inflammasomes Also Drive Regeneration and Fibrosis. *J. Am. Soc. Nephrol.* **2014,** 25, 1387–1400.
9. Sato, Y.; Yanagita, M. Immune cells and inflammation in AKI to CKD progression. *Am. J. Physiol. Renal Physiol.* **2018,** 315, 501–1512.
10. Mack, M.; Yanagita, M. Origin of myofibroblasts and cellular events triggering fibrosis. *Kidney Int.* **2015,** 87, 297–307.
11. Nakamura, J.; Sato, Y.; Kitai, Y., Wajima, S.; Yamamoto, S.; Oguchi, A.; Yamada, R.; Kaneko, K.; Kondo, M.; Uchino, E. Myofibroblasts acquire retinoic acid–producing ability during fibroblast-to-myofibroblast transition following kidney injury. *Kidney Int.* **2019,** 95, 526–539.
12. Kaissling, B.; Lehir, M.; Kriz, W. Renal epithelial injury and fibrosis. *Biochim. Biophys. Acta* **2013,** 1832, 931–939.
13. Zhao, J.; Wang, X.; Wu, Y.; Zhao, C. Kruppel-like factor 4 modulates the miR-101/COL10A1 axis to inhibit renal fibrosis after AKI by regulating epithelial-mesenchymal transition. *Ren Fail.* **2024,** 46, 2316259.
14. Maryam, B., Smith, ME.; Miller, S. J., Natarajan, H., Zimmerman, K.A. Macrophage Ontogeny, Phenotype, and Function in Ischemia Reperfusion-Induced Injury and Repair. *Kidney360.* **2024**, 5, 459-470.

 doi:10.20944/preprints202503.0870.v1

15. Mantovani, A.; Sica, A.; Sozzani, S.; Allavena, P.; Vecchi. A.; Locati. M. The chemokine system in diverse forms of macrophage activation and polarization. *Trends Immunol.* **2004**, 25, 677–686.
16. Guzzi, F.; Cirillo, L.; Roperto, R.M.; Romagnani, P.; Lazzeri, E. Molecular Mechanisms of the Acute Kidney Injury to Chronic Kidney Disease Transition: An Updated View. *Int J Mol Sci.* **2019,** 20, 4941.
17. Kim, D.J.; Kang, J.M.; Park, S.H.; Kwon, H.K.; Song, S.J,.; Moon, H.; Kim, S.M.; Seo, J.W.; Lee, Y.H.; Kim, Y.G; Moon, J.Y,.; Lee, S.Y.; Son, Y.; Lee, S.H. Diabetes Aggravates Post-ischaemic Renal Fibrosis through Persistent Activation of TGF-beta(1) and Shh Signalling. *Sci Rep.* **2017**, 7, 16782.
18. Takai, S.; Shiota, N.; Yamamoto, D.; Okunishi, H.; Miyazaki, M. Purification and characterization of angiotensin II-generating chymase from hamster cheek pouch. *Life Sci.* **1996**, 58, 591–597.
19. Lindstedt, K.A.; Wang, Y.; Shiota, N.; Saarinen, J.; Hyytiäinen, M.; Kokkonen, J.O.; Keski-Oja, J.; Kovanen, P.T. Activation of paracrine TGF-beta1 signaling upon stimulation and degranulation of rat serosal mast cells: a novel function for chymase. *FASEB J.* **2001,** 15, 1377–1388.
20. Zhao, M.; Wang, Y.; Li, L.; Liu, S.; Wang, C.; Yuan, Y.; Yang, G.; Chen, Y.; Cheng, J.; Lu, Y.; Liu, J. Mitochondrial ROS promote mitochondrial dysfunction and inflammation in ischemic acute kidney injury by disrupting TFAM-mediated mtDNA maintenance. *Theranostics* **2021,** 11, 1845–1863.
21. Fan, Y.; Yuan, Y.; Xiong, M.; Jin, M.; Zhang, D.; Yang, D.; Liu, C.; Petersen, R.B.; Huang, K.; Peng, A.; Zheng, L. Tet1 deficiency exacerbates oxidative stress in acute kidney injury by regulating superoxide dismutase. *Theranostics* **2023,** 13, 5348–5364.
22. Nieuwenhuijs-Moeke, G.J.; Pischke, S.E.; Berger, S.P., Sanders , J.S.F.; Pol , R.A.; Struys , M.M.R.F.; Ploeg , R.J.; Leuvnink, H.G.D. Ischemia and reperfusion injury in kidney transplantation: relevant mechanisms in injury and repair. *J Clin Med.* **2020**, 9, 253.
23. Bonventre, J.V.; Yang, L. Cellular pathophysiology of ischemicacute kidney injury. *J Clin Invest.* **2011**, 121:, 4210–4221.
24. Burne-Taney, M.J.; Yokota, N.; Rabb, H. Persistent renal and extrarenal immune changes after severe ischemic injury. *Kidney Int.* **2005,** 67, 1002-1009.
25. Caughey, G.H.; Raymond, W.W.; Wolters, P.J. Angiotensin II generation by mast cell alpha- and beta-chymases. *Biochim Biophys Acta.* **2000**, 1480, 245–257.
26. Andersson, M.K.; Karlson, U.; Hellman, L. The extended cleavage specificity of the rodent betachymases rMCP-1 and mMCP-4 reveal major functional similarities to the human mast cell chymase. *Mol Immunol.* **2008**, 45, 766–775.
27. Griendling, K.K.; Minieri, C.A.; Ollerenshaw, J.D.; Alexander, RW. Angiotensin II stimulates NADH and NADPH oxidase activity in cultured vascular smooth muscle cells. *Circ Res.* **1994**, 74, 1141–1148.
28. Garrido, A.M.; Griendling, K.K. NADPH oxidases and angiotensin II receptor signaling. *Mol Cell Endocrinol.* **2009**, 302, 148–158.
29. Asehnoune, K.; Strassheim, D.; Mitra, S.; Kim, J.Y.; Abraham, E. Involvement of reactive oxygen species in Toll-like receptor 4-dependent activation of NF-kappa B. *J Immunol.* **2004**, 172, 2522–2529.
30. Terai. K.; Jin, D.; Watase, K.; Imagawa, A.; Takai, S. Mechanism of Albuminuria Reduction by Chymase Inhibition in Diabetic Mice. *Int J Mol Sci.* **2020**, 21, 7495.
31. Nishimura, H.; Jin, D.; Kinoshita, I.; Taniuchi, M.; Higashino, M.; Terada, T.; Takai, S.; Kawata, R. Increased Chymase-Positive Mast Cells in High Grade Mucoepidermoid Carcinoma of the Parotid Gland. *Int J Mol Sci.* **2023**, 24, 8267.